2.1 SIMULATION OF AN OZONE EPISODE DURING THE CENTRAL CALIFORNIA OZONE STUDY
PART I: MM5 METEOROLOGICAL MODEL SIMULATIONS

James M. Wilczak[1], Jian-Wen Bao[1], Sara A. Michelson[1], Saffet Tanrikulu[2], and Su-Tzai Soong[2]

[1]NOAA/Environmental Technology Laboratory, Boulder, CO 80305
[2]Bay Area Air Quality Management District, San Francisco, CA 94109

1. INTRODUCTION

The Central California Ozone Study (CCOS 2000) is a combined observational and modeling program designed to improve our understanding of the mechanisms of ozone formation and transport within California. CCOS 2000 was motivated by the fact that ozone concentrations frequently exceed the federal 1- and 8-hour (124 and 84 ppb) standards in central California. During the CCOS 2000 field program, extensive observations of meteorology and air chemistry were collected in central California to document high ozone episodes and the meteorology that was associated with them. The CCOS field program operated from June 1 through October 2, 2000. During this period, several moderate ozone episodes occurred, of which the episode that occurred between July 30-August 2 will be examined in this study.

Goals of CCOS 2000 were to evaluate the meteorological and chemical modeling system used for the state implementation plan (SIP) for this region, and to better understand through numerical modeling the role of various meteorological phenomena in ozone formation, transport and mixing. The meteorological phenomena in the central California region that are known to have a pronounced impact on ozone concentrations include 1) the sea-breeze, which can bring cooler, moister, and less polluted air as it propagates inland; 2) flow through the San Francisco Bay area, which is the principal inflow to the Central Valley, and the split of this flow, which determines the relative inflow into the Sacramento and San Joaquin Valleys; 3) nocturnal low-level jets, which can rapidly transport boundary layer pollutants along the Central Valley; 4) mesoscale eddies (the Schultz, Fresno, and Bakersfield) which can recirculate ozone and its precursors; and 5) slope flows, which result in transport in or out of the valleys, support boundary layer venting along mountain crests, and produce subsidence or ascending motion over the valleys. In addition, the depth of the atmospheric boundary layer is of critical importance for air quality, as it determines the depth through which pollutants are vertically mixed.

To better understand the role of the above meteorological phenomena on ozone transport and mixing, a meteorological and chemical modeling system was used to simulate ozone concentrations. This system was comprised of the MM5 meteorological model, and the CAMx photochemical model. In this paper we present the meteorological modeling results, while in Part II (Soong et al.) the emissions database, photochemical model, and ozone simulations will be presented.

* *Corresponding author address*: James Wilczak, NOAA/ETL; 325 Broadway, Boulder 80305, CO; e-mail:james.m.wilczak@noaa.gov.

2. OBSERVATIONAL DATA

The observational data sets used for the meteorological comparison include 297 surface meteorological stations, 120 surface ozone monitors and network of 25 915 MHz wind profilers. The network of wind profilers (see http://www.etl.noaa.gov/programs/modeling/ccos/data for the site locations) was one of the core sets of meteorological instrumentation used for CCOS 2000. The wind profilers provided hourly averages of wind speed and direction, typically to heights of 3000 m AGL. In addition to winds, the vertical profiles of virtual temperature were measured using the Radio Acoustic Sounding System (RASS) technique, which typically reached heights of 1000 m AGL. The depth of the daytime, convective ABL was also determined from the wind profiler measurements by visually inspecting values of range-corrected signal to noise ratio, vertical velocity (which is large within the convective ABL), and radar spectral width (which is a measure of turbulence intensity) (White, 1993; Angevine et al., 1994; Bianco and Wilczak, 2002).

3. MODEL DESCRIPTION AND CASE STUDY CHARACTERIZATION

The high ozone episode discussed in this paper occurred from 30 July to 02 August, 2000. During this period, the synoptic meteorology was characterized by a ridge at 500 mb that started to regress toward the west from New Mexico and strengthened on July 27. During the Intensive Operational Period (IOP) of July 30 -August 2, the ridge remained strong and continued to slowly regress toward the west so that by July 31 it was centered near Reno, Nevada. The 850 mb temperature at Oakland reached as high as 27^{o}C and the 500 mb height peaked at 5,970 m. At the surface, high pressure was present over the Great Basin area with its center located to the northeast of the San Joaquin Valley, rendering a weak off-shore pressure gradient between San Francisco and Reno and a weak north-to-south gradient from San Francisco to Las Vegas. Under such a synoptic pattern, the low-level winds were weak and the sky was mostly cloud free over the San Joaquin Valley, a condition conducive to high ozone events.

MM5 simulations for this episode were run using a 36-12-4 km one-way nested model domain. The model domain had 50 vertical stretched levels among which 30 were within the lowest 2 km and the lowest model level was at about 12 m above the surface. The 4 km domain encompasses the CCOS field study area, which extends from the Pacific Ocean in the west to the Sierra Nevada in the east, and from Redding, CA, in the north to the Mojave Desert in the south. Boundary and initial conditions were prescribed using the 6-hourly 40 km NCEP Eta analysis. The simulations began at 12 UTC 29 July, and were run for 120 h, ending at 12 UTC 3 August 2000.

Various MM5 simulations were run testing different combinations of surface and boundary layer parameterizations and land surface models. Comparing these simulations with observations indicates that the most overall accurate simulation was produced when using the Eta planetary boundary layer and surface layer schemes, and the NOAH land surface model (LSM). In addition, this simulation used the Reisner microphysics parameterization, and the Dudhia short-wave and RRTM long-wave radiation parameterizations. The Grell convective parameterization scheme was used on the 36 and 12 km grids. No convective parameterization scheme was used on the 4 km grid. We will refer to this simulation as Run 1.

It is a common practice in air quality modeling for SIPs to assimilate observations into the meteorological model using the nudging FDDA technique in order to obtain the most realistic meteorological forcing of the photochemical model. Thus, a second MM5 simulation was run differently than Run 1, in that it used analysis nudging on the 36 km domain and observational nudging of the profiler and surface winds on the 4 km domain. We will refer to this run as Run 2. In this FDAA run, a nudging term is added to the prognostic equations of wind and temperature, such that the model state is gradually “nudged” toward the observations based on the difference between the two (see, e.g., Stauffer and Seaman, 1994). In order to illustrate the impact that the LSM and FDDA have on the accuracy of the model simulation, we include in the study a run (Run 3) that is the same as Run 1 except a simple 5-layer soil model was used instead of the LSM.

4. RESULTS OF COMPARISON

In this paper, direct comparisons between the observations and the model output at the observational sites are presented. Because the highest ozone concentration within the San Francisco Bay Area during this 5 day episode occurred on 31 July (Julian Day 213), and the photochemistry for this day is examined in detail in Part II, we focus on the direct meteorological evaluation on this day. In addition, we limit our surface observation comparisons to the San Joaquin Valley and the San Francisco Bay Area, and the wind profiler comparisons to profilers located in Richmond (in the San Francisco Bay Area), Sacramento, and Bakersfield, because these are the areas that have ozone violations during this IOP.

Figure 1 shows 24 h time-height cross-sections of winds and virtual temperature from the wind profiler and RASS at Richmond, and the corresponding output from Run 1 and Run 2. It can be seen that during the entire 24-h period, the simulated winds from Run 1 and the observed winds show a similar transition from westerly to northerly to northeasterly and back to westerly at 500m AGL. However, there are noticeable differences between the simulated and the observed winds. From 0000 UTC to 0500 UTC, the observed winds are more northwesterly than the simulated winds in Run 1. From 1400 UTC to 1900 UTC the observations show northwesterly winds within the lowest few hundred meters. The simulated winds in Run 1 do not have this northwesterly flow during this time. Similar to Run 1, Run 2 captures the general transition of the winds throughout this 24-h period. However, from

0000 UTC to 500 UTC, the simulated winds in Run 2 are more northwesterly than in Run1, which is in better agreement with the observations than Run 1. Additionally, in Run 2 the northwesterly flow between 1400 and 1900 UTC is better simulated than in Run 1. Despite the overall positive impact of FDDA, the observed northeasterly flow between 1600 UTC and 2000 UTC between 0.3 km and 1.5 km is better simulated by Run 1 than Run 2. When compared with the RASS data, both Run 1 and Run 2 appear to be colder during the entire 24 h period than the observations, but Run2 is generally warmer than Run 1, indicating the impact of FDDA of the observed winds on the simulated temperature.

Figure 2 is the same as Fig. 1, except for the Sacramento site. It can be seen that the simulated winds from Run 1 show a persistent westerly flow below 0.25 km through the entire 24-h period, but in the observations the westerly winds shift to north/northeasterly at 0700 UTC, and shift back to westerly at 1800 UTC. The winds from Run 2 are also persistent westerly in the lowest 0.25 km, but the depth and the intensity of the westerly flow is weaker in Run 2 than Run 1 from 0700 UTC to 1800 UTC. This indicates the positive impact of FDDA because the observations show weaker winds than what were simulated in Run 1. It is interesting that at this site, FDDA of the observed winds not only improved the simulated winds, but also improved the simulated virtual temperature, except near the surface during the night.

At the Bakersfield wind profiler site, the simulated winds from Run 1 show a significant difference at lower levels (below 0.5 km) than the observed from 0400 UTC to 1800 UTC. The simulated winds are southerly and much stronger than observed. The simulated winds from Run 2 are in much better agreement with the observations than Run 1 due to the positive impact of FDDA. The simulated temperature from Run 1 is slightly cooler than the observed, while the temperature from Run 2 is warmer than Run 1, especially during the nighttime hours, due to the impact of FDDA of the observed winds.

Figures 4-7 show the areal average, time-series plots of the direction and speed of the observed surface winds as well as the observed surface temperature and dew-point temperature, along with the simulated counterparts from Run 1 and Run 2. The areal average was performed over the San Francisco Bay Area (area 3), and the northern (area 5), the central (area 6) and the southern (area 7) San Joaquin Valley. The mean and absolute biases are given for each area along with the standard deviation. In the wind comparison, we compare wind speed as well as wind direction because the latter is perhaps the most important meteorological parameter for air quality prediction, as it determines the trajectory of pollutant plumes emanating from urban areas or point sources.

The mean and absolute biases vary from one area to another. In the San Francisco Bay area (Fig. 4), the winds from Run 1 show a similar diurnal cycle as was observed, but with significant discrepancies in wind speed and direction, in particular during the last 3 days of the simulation period. FDDA of the observed winds not only improved both wind speed and direction, but also had an overall positive impact on the surface temperature and dew-point temperature. In the three areas of the San Joaquin Valley (areas 5, 6 and 7), the errors in the winds from Run 1 (Figs. 5-7) are greater than those in the San Francisco Bay Area (Fig. 4), and it is expected that FDDA would have more impact in these three areas than the San Francisco Bay Area. Indeed, FDDA significantly improved the wind speed and direction as indicated by the time-series comparison and the numbers of the mean and absolute biases corresponding to Run 1 and Run 2. However, although FDDA improved the simulated surface temperature and dew-point temperature from Run 2 in area 5, the mean and absolute biases indicate that it made the simulation of the surface temperature and dew-point temperature slightly worse in both areas 6 and 7 than Run 1.

From comparisons of the results of Run 1 and Run 2 with the observations, it is clear that the FDDA of the observed winds has a significant, overall positive impact on the simulation of both wind and temperature. To shed light on the impact that the LSM has on the accuracy of the model simulation relative to FDDA, Run1 and Run 3 are compared to the observations. Figures 8-11 show the same areal comparison as in Figs. 4-7, except for the comparisons of Run 1 and Run 3 with the observations. By examining the mean and absolute biases of Run 1 and Run 3 with the observations, it is obvious that although the use of the LSM generally improved the surface temperature and moisture, it increased the biases in both the wind speed and wind direction. This result is important because it indicates that the simple 5-layer soil model was not sufficient to accurately simulate the surface temperature and moisture. Although the use of the more realistic LSM significantly improved the surface temperature and moisture, the wind simulation was somewhat degraded by using the LSM in terms of the mean and absolute biases. Therefore, in order to improve the wind simulation when using the LSM, FDDA of the observed winds was required.

Finally, in Fig. 12 we show the observed and simulated boundary layer depths, averaged over the central portion of the Central Valley, including Sacramento. Both Run 1 and Run 2 agree quite well with the observed ABL depths, when averaged over the entire IOP. On 31 July (JD213), the second full day shown in the figure, the both model simulations also agree very well with the observations. In most other regions of the analysis domain good agreement was found between the observations and model. An exception was for profiler sites immediately inland of the San Francisco Bay Area (Livermore and San Martin sites) where the model frequently produces boundary layer depths that are too low.

3. SUMMARY AND CONCLUSIONS

A case study was carried out in which the output from the combined meteorology and chemistry modeling system for California's SIPs was compared with the wind profiler/RASS and surface observations of both wind and temperature. The meteorological model was run on a 36-12-4 km one-way nested model domain of 50 vertical levels, with the 4 km domain encompassing the CCOS 2000 field study area. Among various MM5 simulations of the chosen case with different combinations of surface and boundary layer parameterizations and land surface models, we found that overall the most accurate simulation was produced when using the Eta planetary boundary layer and surface layer schemes, the NOAH land surface model (LSM) and FDDA.

The direct meteorological comparison between the model simulation and the observations from the CCOS 2000 field experiment indicates that the errors in the simulated low-level winds and surface temperature varied from one area to another, although the model simulated large-scale pattern was in fairly good agreement with the analysis. Generally, the simulated low-level winds and surface temperature were in better agreement with the observations in San Joaquin Valley than the coastal areas. The use of the NOAH LSM led to more accurate simulations of surface temperature and moisture. FDDA of the observed winds significantly improved the simulated wind field, and reduced the cold bias in the simulated temperature field. Good agreement was found between the area-average observed and simulated ABL heights except for the area immediately inland such as the San Francisco Bay Area.

4. REFERENCES

Angevine, W. M., A. B. White, and S. K. Avery, 1994: Boundary-layer depth and entrainment zone characterization with a boundary-layer profiler, *Boundary-Layer meteorol*., **68,** 375-385.

Bianco, L., and Wilczak, J. M., 2002: Convective boundary layer depth: Improved measurement by Doppler radar wind profiler using fuzzy logic methods, *J. Atmos. Oceanic Technol.*, **19**, 1745–1758.

Weber and Wuertz (1992)

White, A. B., 1993: Mixing depth detection using 915-MHz radar reflectivity data, *Preprints, Eighth Symp. On Observations and Instrumentation*, Anaheim, Califonia, Amer. Meteor. Soc., 248-250.

Wilczak, J. M., R. G. Strauch, F. M. Ralph, B. L. Weber, D. A. Merritt, J. R. Jordan, D. E. Wolfe, L. K. Lewis, D. B. Wuertz, J. E. Gaynor, S. A. McLaughlin, R. R. Rogers, A. C. Riddle, and T. S. Dye, 1995: Contamination of wind profiler data by migrating birds: characteristics of corrupted data and potential solutions, *J. Atmos. Oceanic Technol*., **12**, 449-467.

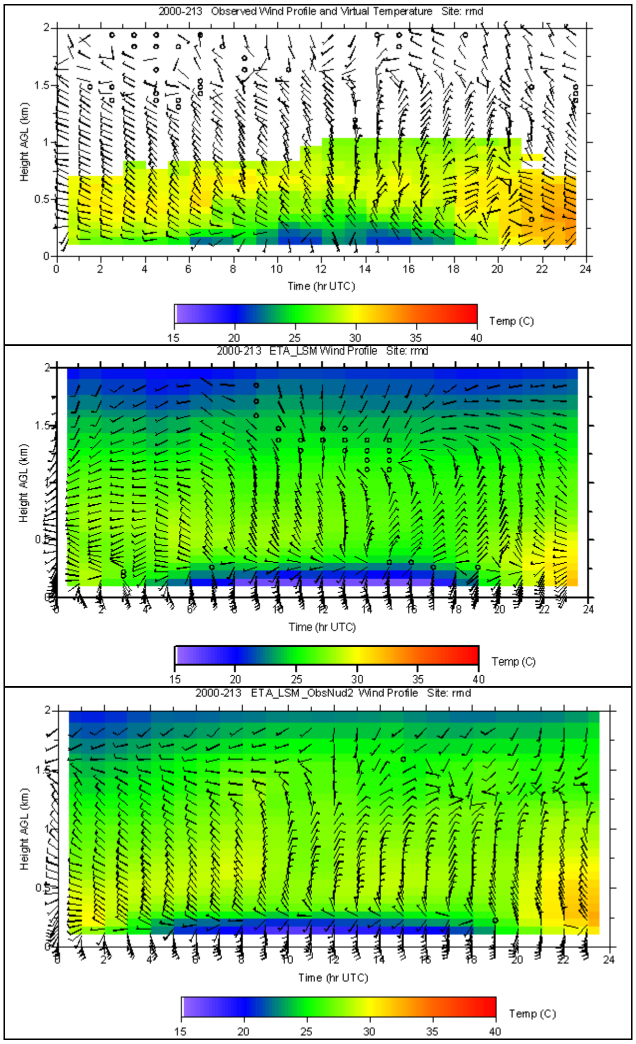

Figure 1. Time-height cross-sections of virtual temperature (°C) and winds at the Richmond profiler site on JD 213. Top panel shows the observations, middle panel Run 1, and bottom panel Run 2.

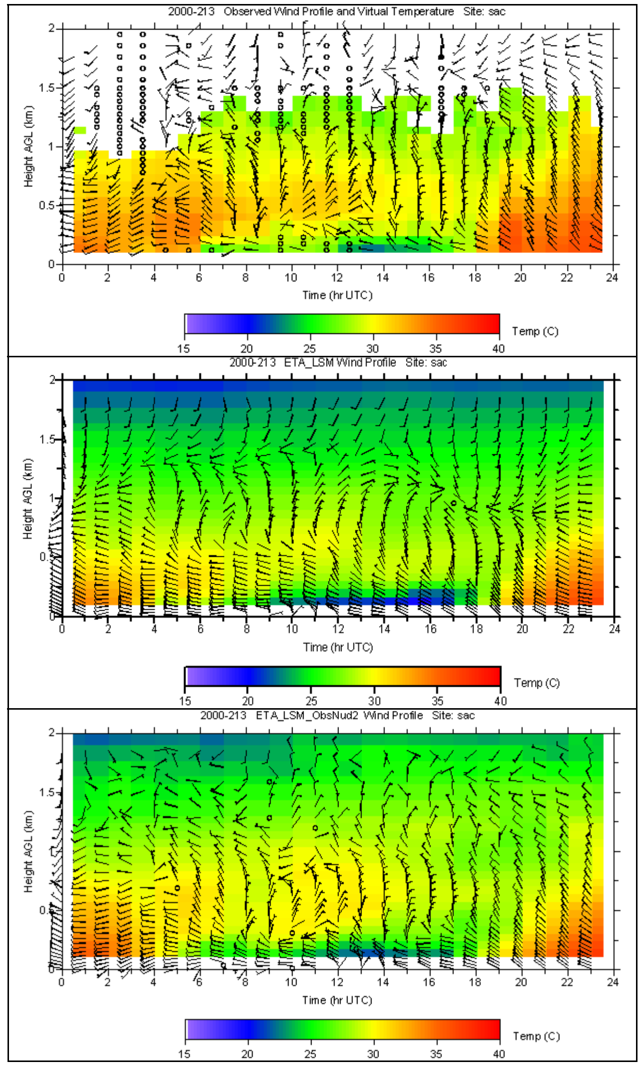

Figure 2. Time-height cross-sections of virtual temperature (°C) and winds at the Sacramento profiler site on JD 213. Top panel shows the observations, middle panel Run 1, and bottom panel Run 2.

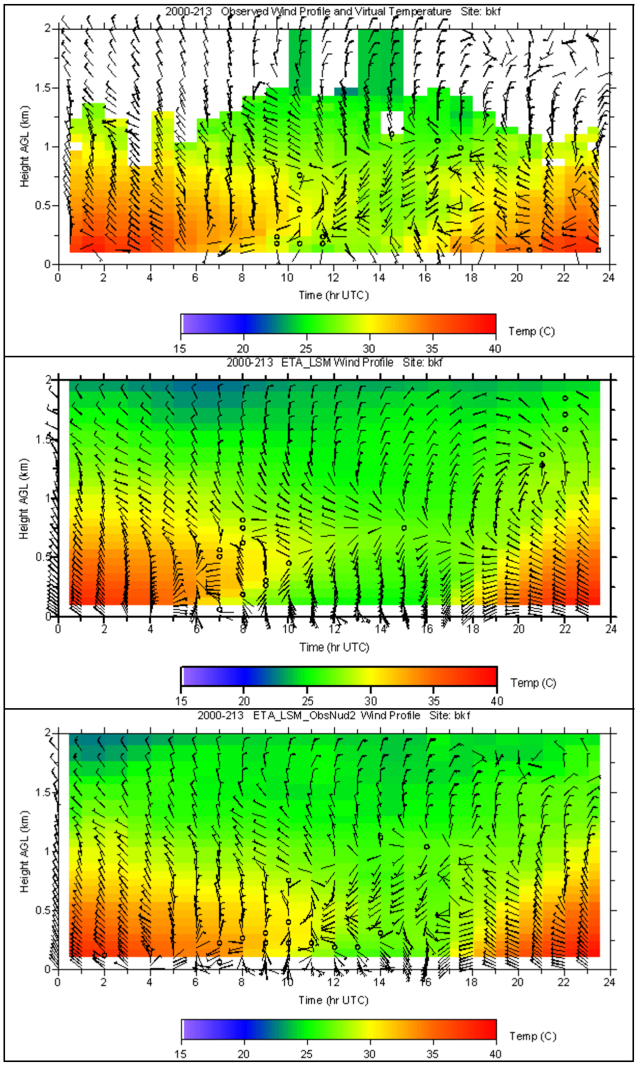

Figure 3. Time-height cross-sections of virtual temperature (°C) and winds at the Bakersfield profiler site on JD 213. Top panel shows the observations, middle panel Run 1, and bottom panel Run 2.

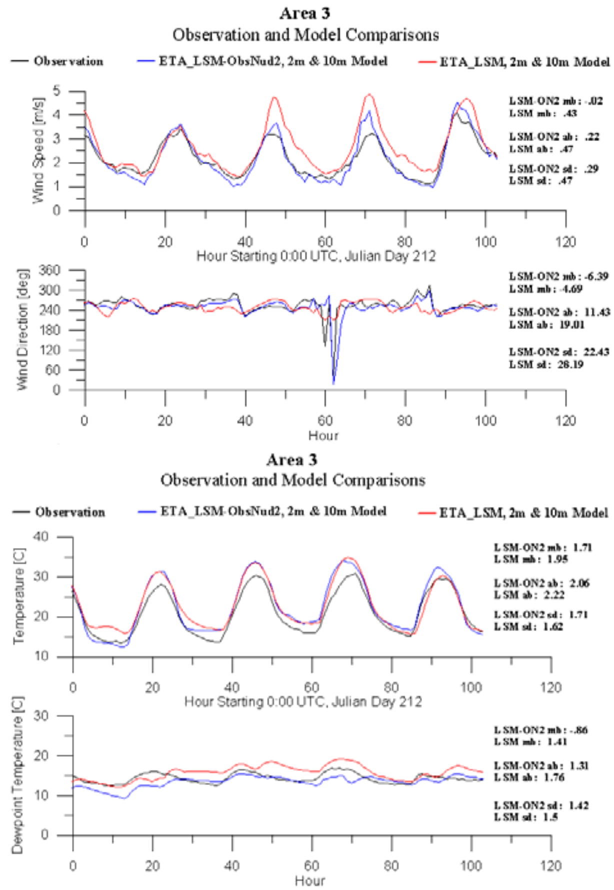

Figure 4. Time series of the Area 3 (San Francisco Bay area) averages surface meteorology that are arranged from the top panel down: 10-m wind speed (ms^{-1}); 10-m wind direction; 2-m temperature (°C); and 2 m dewpoint temperature (°C). Black line is the observed average, red line is the Run1 average and the blue line is the Run 2 average.

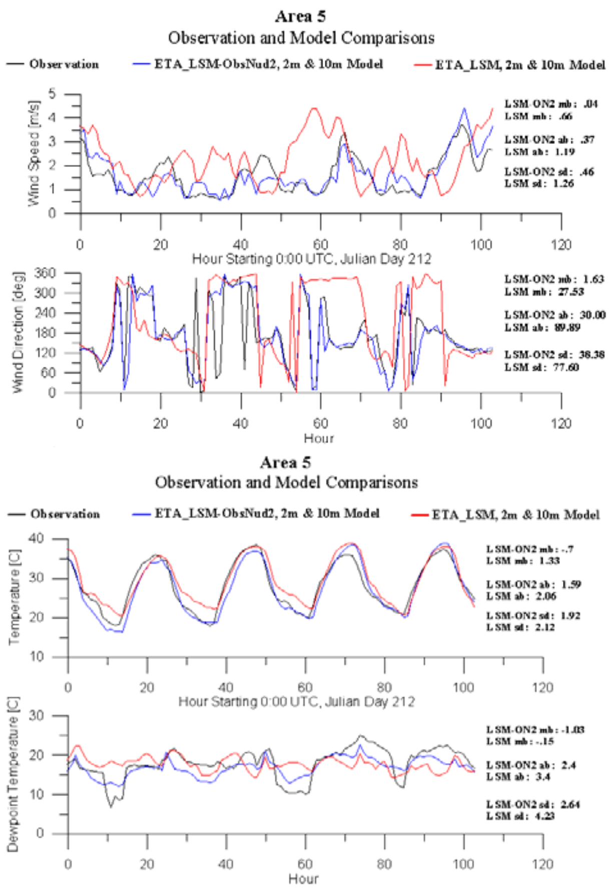

Figure 5. The same as Fig. 4, but for the Area 5 (the northern San Joaquin Valley).

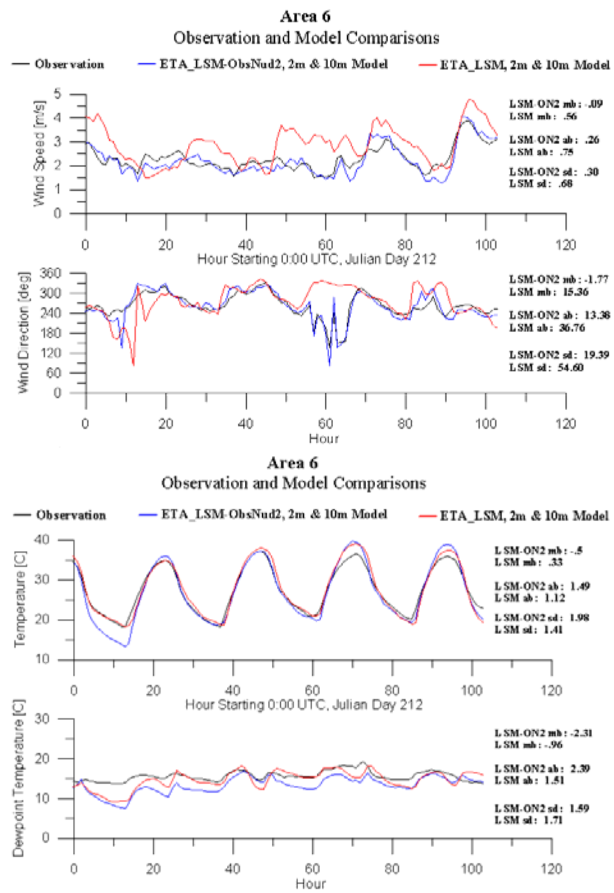

Figure 6. The same as Fig. 4, but for the Area 6 (the central San Joaquin Valley).

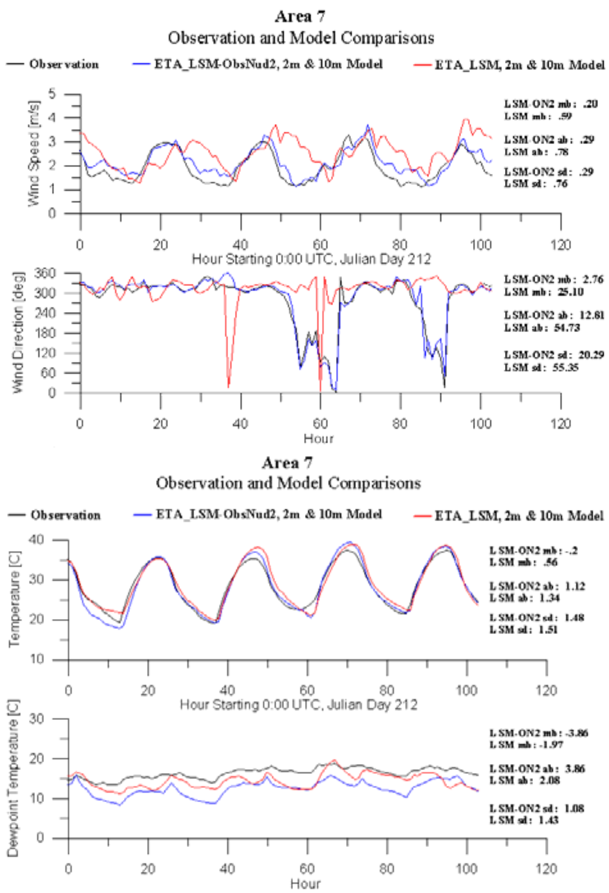

Figure 7. The same as Fig. 4, but for the Area 7 (the southern San Joaquin Valley).

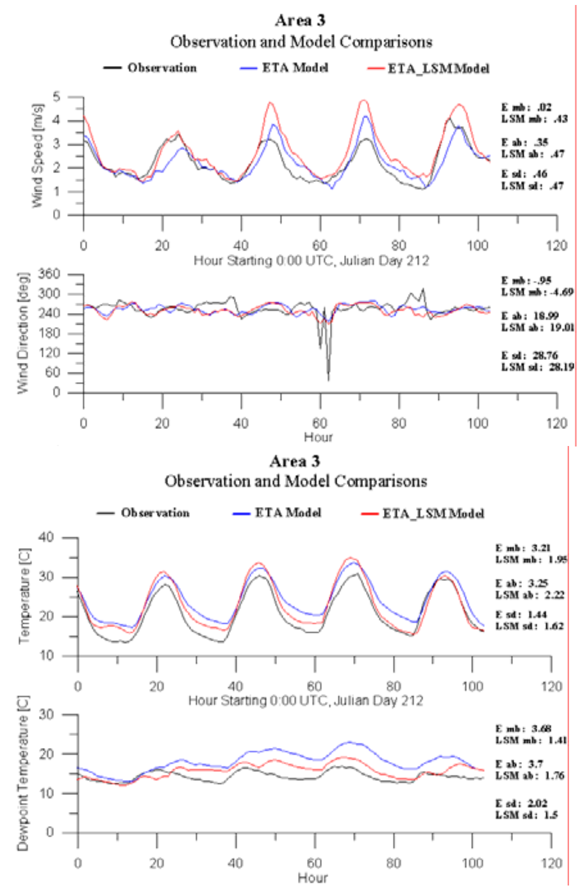

Figure 8. Time series of the Area 3 (San Francisco Bay area) averaged surface meteorology that are arranged from the top panel down: 10-m wind speed (ms^{-1}); 10-m wind direction; 2-m temperature (°C); and 2 m dewpoint temperature (°C). Black line is the observed average, red line is the Run1 average and the blue line is the Run 3 average.

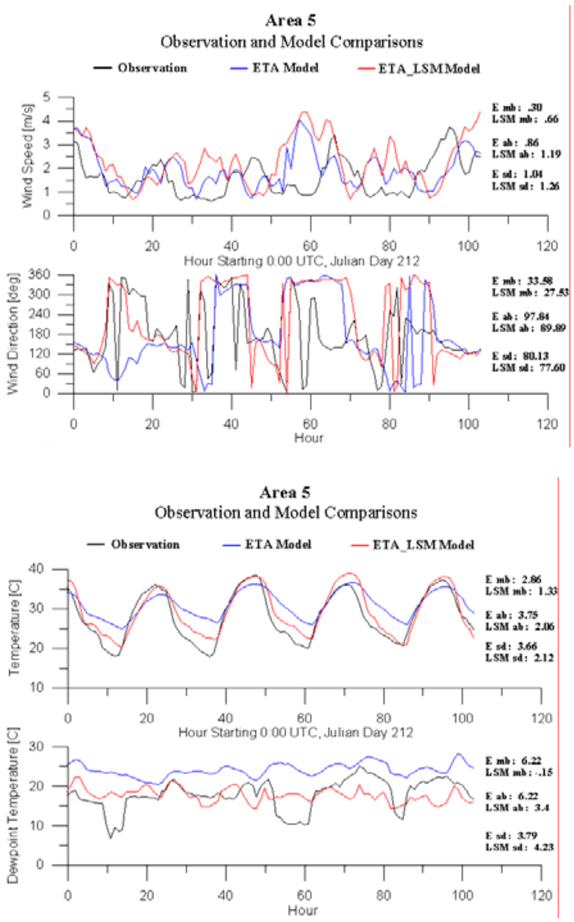

Figure 9. The same as Fig. 8, but for the Area 5 (the northern San Joaquin Valley).

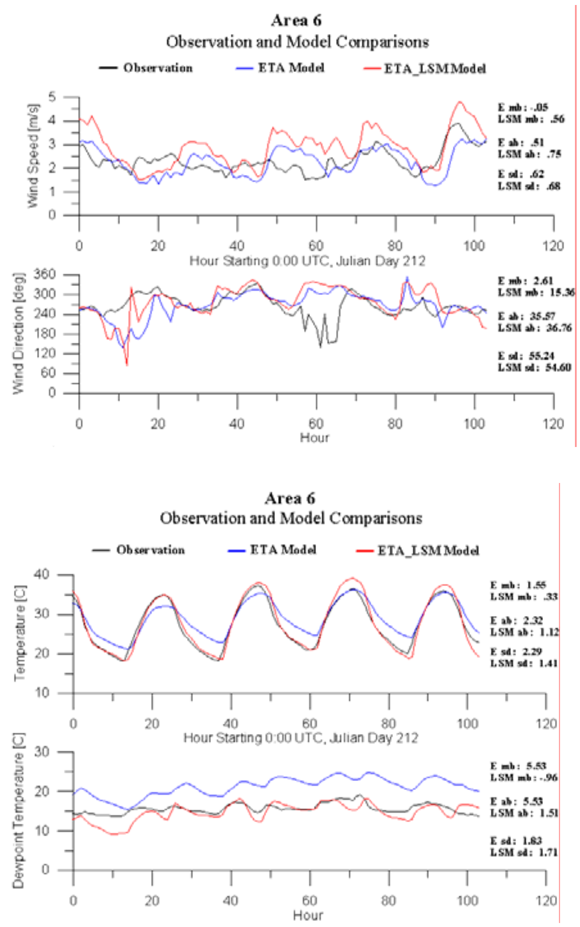

Figure 10. The same as Fig. 8, but for the Area 6 (the central San Joaquin Valley).

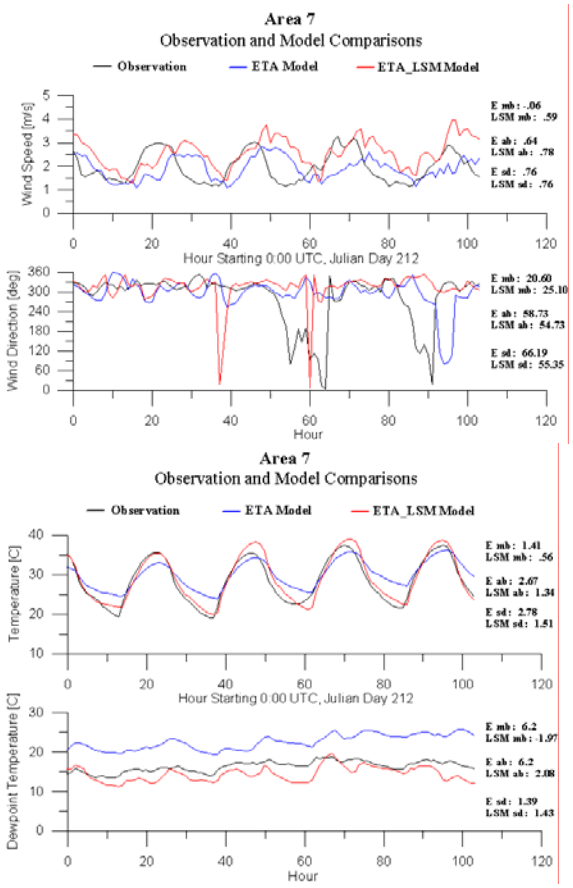

Figure 11. The same as Fig. 8, but for the Area 7 (the southern San Joaquin Valley).

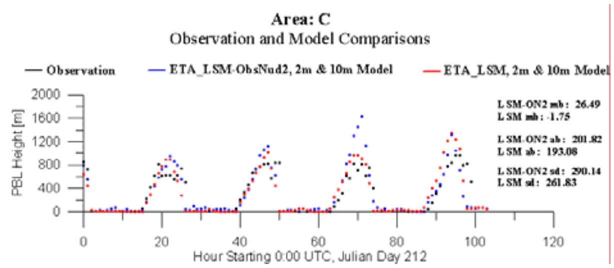

Figure 12. The observed and simulated boundary layer depths from Run1 and Run2, averaged over the central portion of the Central Valley.